AGU PUBLICATIONS

JGR

Journal of Geophysical Research: Atmospheres

RESEARCH ARTICLE
10.1002/2016JD026019

Key Points:
- Cloud water sea salt and near-surface giant particle concentrations are related and represent GCCN in the marine atmosphere
- Clouds with higher chloride concentrations coincide with enhanced rain rate (at fixed LWP) and negative precipitation susceptibility values
- Differences in vertical drop size data between low and high chloride cases suggest GCCN-produced raindrops precipitate before reaching tops

Correspondence to:
A. Sorooshian,
armin@email.arizona.edu

Citation:
Dadashazar, H., Z. Wang, E. Crosbie, M. Brunke, X. Zeng, H. Jonsson, R. K. Woods, R. C. Flagan, J. H. Seinfeld, and A. Sorooshian (2017), Relationships between giant sea salt particles and clouds inferred from aircraft physicochemical data, *J. Geophys. Res. Atmos.*, *122*, 3421–3434, doi:10.1002/2016JD026019.

Received 30 SEP 2016
Accepted 2 MAR 2017
Accepted article online 8 MAR 2017
Published online 20 MAR 2017

Relationships between giant sea salt particles and clouds inferred from aircraft physicochemical data

Hossein Dadashazar[1], Zhen Wang[1], Ewan Crosbie[2,3], Michael Brunke[4], Xubin Zeng[4], Haflidi Jonsson[5], Roy K. Woods[5], Richard C. Flagan[6], John H. Seinfeld[6], and Armin Sorooshian[1,4]

[1]Department of Chemical and Environmental Engineering, University of Arizona, Tucson, Arizona, USA, [2]NASA Langley Research Center, Hampton, Virginia, USA, [3]Universities Space Research Association, Columbia, Maryland, USA, [4]Department of Hydrology and Atmospheric Sciences, University of Arizona, Tucson, Arizona, USA, [5]Naval Postgraduate School, Monterey, California, USA, [6]Department of Chemical Engineering, California Institute of Technology, Pasadena, California, USA

Abstract This study uses airborne data from multiple field campaigns off the California coast to determine the extent to which a size distribution parameter and a cloud water chemical measurement can capture the effect of giant cloud condensation nuclei (GCCN), specifically sea salt, on marine stratocumulus cloud properties. The two GCCN proxy variables, near-surface particle number concentration for diameters >5 μm and cloud water chloride concentration, are significantly correlated (95% confidence) with each other, and both exhibit expected relationships with other parameters (e.g., surface wind) that typically coincide with sea salt emissions. Factors influencing the relationship between these two GCCN proxy measurements include precipitation rate (*R*) and the standard deviation of the subcloud vertical velocity owing likely to scavenging effects and improved mixing/transport of sea salt to cloud base, respectively. When comparing 12 pairs of high and low chloride cloud cases (at fixed liquid water path and cloud drop number concentration), the average drop spectra for high chloride cases exhibit enhanced drop number at diameters exceeding 20 μm, especially above 30 μm. In addition, high chloride cases coincide with enhanced mean columnar *R* and negative values of precipitation susceptibility. The difference in drop effective radius between high and low chloride conditions decreases with height in cloud, suggesting that some GCCN-produced raindrops precipitate before reaching cloud tops. The sign of cloud responses (i.e., *R*) to perturbations in giant sea salt particle concentration, as evaluated from Modern Era Retrospective Analysis for Research and Applications version 2 reanalysis data, is consistent with the aircraft data.

1. Introduction

A long-standing issue in understanding warm cloud formation and dynamics is the role of extremely large hygroscopic nuclei, commonly referred to as giant cloud condensation nuclei (GCCN). The minimum diameter threshold for GCCN is widely defined, ranging in the literature from 1 to 20 μm [e.g., *Johnson*, 1982; *Pruppacher and Klett*, 1997; *Jensen and Lee*, 2008]. The upper size limit of GCCN has received less attention, although their diameters have been noted to reach as high as 300 μm [*Laird et al.,* 2000]. Several decades ago, it was proposed that GCCN expedite warm rain initiation by promoting the formation of large drops and enhancing the collision-coalescence process [*Houghton*, 1938]. Numerous studies have since attempted to increase our understanding of GCCN-cloud interactions, including studies on (i) emissions and vertical profiles of GCCN types such as sea salt [*Woodcock and Gifford*, 1949; *Woodcock*, 1953; *Laird et al.,* 2000]; (ii) drop size distributions, the collision-coalescence process, and precipitation formation [*Woodcock et al.,* 1971; *Takahashi*, 1976; *Ochs and Semonin*, 1979; *Johnson,* 1982; *Mather*, 1991; *Johnson*, 1993; *Feingold et al.,* 1999; *Szumowski et al.,* 1999; *Yin et al.,* 2000; *Rosenfeld et al.,* 2002; *Zhang et al.,* 2006; *Jensen and Lee*, 2008; *Sorooshian et al.,* 2013; *Jung et al.,* 2015]; (iii) cloud thickness [*L'Ecuyer et al.,* 2009]; (iv) radar echoes [*Lasher-Trapp et al.,* 2001; *Knight et al.,* 2002]; and (v) cloud albedo [*Feingold et al.,* 1999]. However, uncertainty remains in the magnitude of these processes and effects. Some studies have shown that GCCN have a very small, or even negligible, impact on initiation of rain in warm clouds owing to both other significant factors at work and that their effect may only be evident under specific circumstances [*Dagan et al.,* 2015, and references therein]. While observational approaches are anticipated to help in quantifying the role of GCCN, a considerable inventory of archived data exists from which the role of GCCN could potentially be extracted. Airborne data are arguably best suited for such data analysis efforts owing to the ability to collect in situ measurements below and inside clouds.

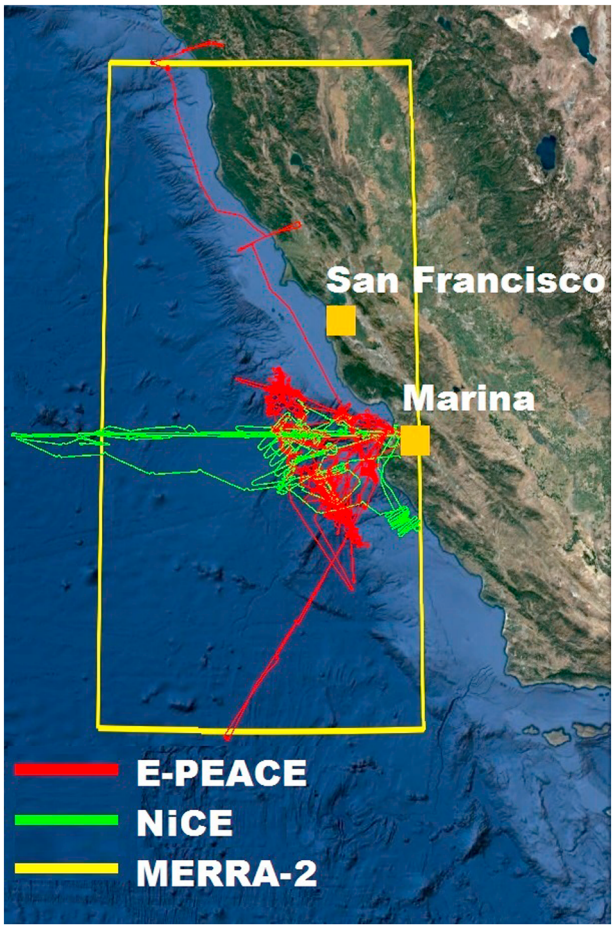

Figure 1. Map showing flight tracks during E-PEACE and NiCE including 14 and five research flights, respectively, from which data are used in this study. Also shown as the yellow rectangle is the spatial area over which MERRA-2 data are analyzed.

GCCN measurements are challenging owing to low number concentrations and instrumental limitations. Some of the earliest measurements from airborne platforms relied on collection rods protruding out of aircraft [e.g., *Woodcock and Gifford*, 1949]. The Giant Nuclei Impactor method is based on collection of GCCN on glass slides exposed to ambient air [e.g., *Colon-Robles et al.,* 2006]. Subcloud number concentration measurements using cloud probes such as the Forward Scattering Spectrometer Probe (FSSP) and Cloud Aerosol Spectrometer (CAS) have been used to detect the possible presence of GCCN using minimum cutpoint diameters as low as 2 μm [*Colon-Robles et al.,* 2006; *Sorooshian et al.,* 2015]. Results of such efforts in marine atmospheres have pointed to a positive association between GCCN number concentration and both wind speed [*Woodcock*, 1953; *Mason*, 2001; *Lewis and Schwartz*, 2004, and references therein] and proximity to major container ships, owing to a combination of influence from their exhaust and wake [*Sorooshian et al.*, 2015].

There are three major goals for the present work. The first aim is to evaluate two potential proxy measurements representative of GCCN in the marine boundary layer using aircraft data. The second goal is to examine interrelationships between the two GCCN proxies, meteorology, and cloud properties. If relationships are extracted that confirm previously reported results, this would provide additional support for the use of the proxy variables. As many past studies of GCCN effects have been based on modeling, having experimental field confirmation would serve as useful validation of modeling results. The last goal is to analyze if similar interrelationships between GCCN and cloud properties emerge in data from a recent reanalysis. Overall, the present study is intended to provide guidance for future field projects, data analysis, and modeling studies focused on GCCN and cloud microphysics.

2. Experimental Methods

Airborne data relevant to stratocumulus clouds are used from four field experiments based out of Marina, California, using the Center for Interdisciplinary Remotely-Piloted Aircraft Studies Twin Otter. The first Marine Stratus/Stratocumulus Experiment (MASE-I) [*Lu et al.,* 2007] included 13 flights in July 2005, the second Marine Stratus/Stratocumulus Experiment (MASE-II) [*Lu et al.,* 2009] included 16 research flights in July 2007, the Eastern Pacific Emitted Aerosol Cloud Experiment (E-PEACE) [*Russell et al.,* 2013] included 30 flights between July and August in 2011, and the Nucleation in California Experiment (NiCE) [*Coggon et al.,* 2014; *Crosbie et al.,* 2016] included 23 flights between July and August in 2013.

During these experiments, the Twin Otter conducted ~4–4.5 h flights at an airspeed of ~50 m s^{-1} in the area encompassed by 34°N–40°N and 121.5°W–125°W (Figure 1) with nearly the same payload. Particle number concentrations in the different size ranges were measured with a condensation particle counter (CPC 3010; TSI Inc.; $D_p > 10$ nm), a passive cavity aerosol spectrometer probe (PCASP; $D_p \sim 0.1$–2.6 μm), and a scanning

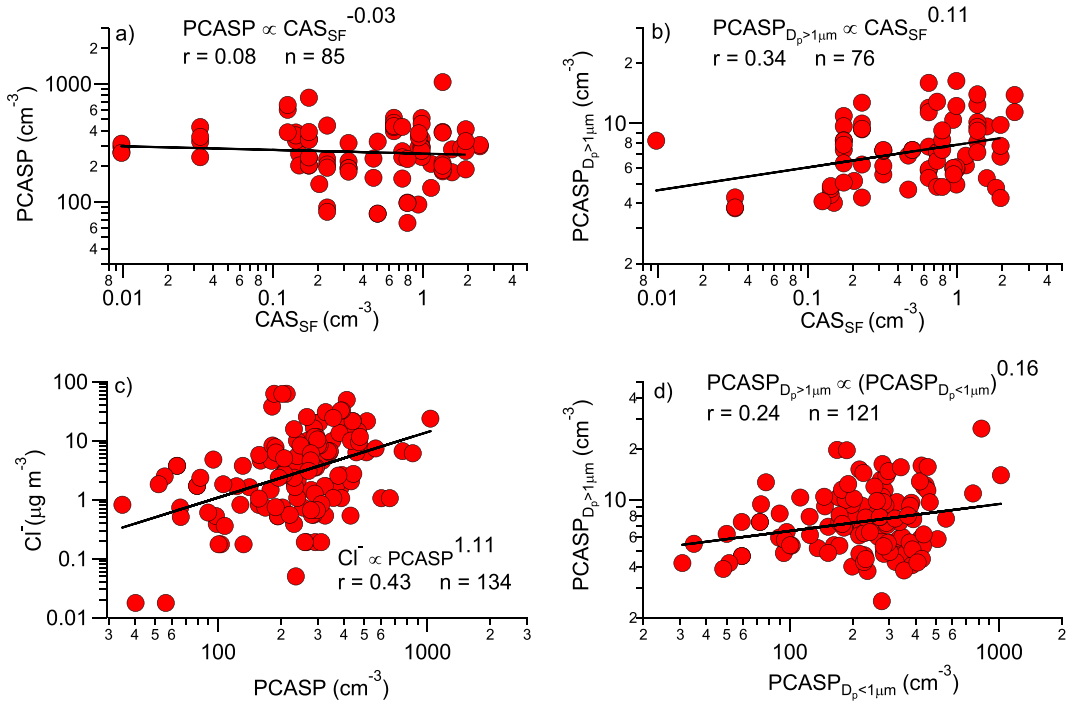

Figure 2. Relationship between (a) subcloud total PCASP concentration and CAS_{SF}, (b) subcloud PCASP concentration for diameters above 1 μm ($PCASP_{Dp>1\,\mu m}$) and CAS_{SF}, (c) cloud water Cl^- and subcloud total PCASP concentration, and (d) subcloud $PCASP_{Dp>1\,\mu m}$ concentration and subcloud PCASP concentration for diameters below 1 μm ($PCASP_{Dp<1\,\mu m}$). These results are based on data from the E-PEACE and NiCE campaigns, with MASE I /II data additionally included in Figures 2a, 2b, and 2d.

mobility particle sizer (D_p ~ 15 nm–800 nm) comprising a differential mobility analyzer (DMA Model 3081, TSI Inc.) coupled to a CPC (Model 3010, TSI Inc.). Droplet size distributions were obtained with a cloud aerosol spectrometer (CAS; D_p ~ 0.6–60 μm), a forward scattering spectrometer probe (FSSP; D_p ~ 2–46 μm), and a cloud imaging probe (CIP; D_p ~ 25–1550 μm). Basic meteorological data were recorded (e.g., temperature, humidity, and winds).

During E-PEACE and NiCE, cloud water was collected with a Mohnen slotted-rod collector [*Hegg and Hobbs*, 1986]. Details about the collection, storage, and chemical analyses of cloud water from E-PEACE and NiCE are provided elsewhere [*Prabhakar et al.,* 2014; *Wang et al.,* 2014]. Briefly, samples were collected over an ~10–30 min duration in high-density polyethylene bottles. Samples were analyzed for pH (Oakton Model 110 pH meter calibrated with pH 4.01 and pH 7.00 buffer solutions), water-soluble composition (Ion Chromatography, IC; Thermo Scientific Dionex ICS—2100 system) and elemental composition (inductively coupled plasma–mass spectrometry, ICP-MS; Agilent 7700 Series). Liquid-phase concentrations of cloud water species were converted to air-equivalent concentrations based on the average cloud liquid water content (LWC), as measured by a PVM-100 probe [*Gerber et al.,* 1994], during the cloud water collection time. A threshold LWC value of 0.02 g m^{-3} is used to distinguish between cloud and cloud-free air, as has been done previously for the study region [*Wang et al.,* 2016]. Of relevance to this study are sodium (Na) and chloride (Cl^-) measured by ICP-MS and IC, respectively. Sodium data from ICP-MS (Na) offered better data quality as compared to IC (Na^+), and it is assumed that Na is predominantly in the form of sea salt in the study region. The collector has little correlation with drop diameter up to a mass mean diameter of approximately 35 μm [*Hegg and Hobbs*, 1986]. Drops during E-PEACE and NiCE flights were sampled with variable size-dependent collection efficiencies. While the majority of the focus here is on E-PEACE and NiCE owing to availability of cloud water data, the MASE experiments are included for additional statistics in some of the selected analyses discussed, specifically Figures 2a, 2b, and 2d, that do not involve cloud water data.

The general flight pattern used in these campaigns was as follows: level legs below cloud base, immediately above cloud base, at midcloud altitude, immediately below cloud top, immediately above cloud top (called

"wheels-in" leg), and a few hundred feet above cloud top as part of a "free troposphere" leg. Vertical soundings, either as slants or spirals, were typically conducted before and/or after each of these sets of leg patterns, from which column-integrated and mean columnar values could be calculated. Cases of clouds decoupled from the surface layer, as identified by discontinuities in thermodynamic variables from vertical sounding data (see details in *Wang et al.* [2016]), are removed as those clouds are less influenced by GCCN emissions from the surface. Details of calculations of cloud parameters such as liquid water path (LWP), drop effective radius (r_e), and rain rate (R) are summarized in past studies [e.g., *Duong et al.,* 2011; *Chen et al.,* 2012; *Crosbie et al.,* 2016]. Vertically resolved and mean columnar R were calculated using CIP data during vertical profiles with the assumption of homogeneous clouds for which there is no spatial variability in drop size distribution (and therefore liquid water content) and using relationships between drop size and fall velocity summarized elsewhere [e.g., *Feingold et al.,* 2013]. Depending on the availability of either the FSSP or CAS during a particular campaign, one of them was used to calculate vertically resolved and mean columnar r_e, which is the ratio of the third to the second moment of the drop size distribution. LWP is calculated with the vertical integration of LWC as measured by the PVM-100 probe. In the subsequent discussion of measurement data results, individual data points represent the average of 1 Hz data from the aforementioned instruments (e.g., FSSP, CAS, CIP, PCASP, and PVM-100) at the specific altitude or altitude range of the parameter being shown.

3. Results and Discussion

3.1. Evaluation of GCCN Proxies

As noted earlier, there are varying reports in the literature for the exact diameter range for particles to qualify as GCCN. A major source of GCCN in the study region is sea salt [*Wang et al.,* 2014; *Modini et al.,* 2015]. Size-resolved aerosol measurements in the study region during NiCE showed that both Cl^- and Na peak in mass concentration between aerodynamic diameters of 1 and 10 μm [*Maudlin et al.,* 2015]. As a result, we use both size distribution data above 1 μm and measurements of Cl^- and Na to deduce GCCN influence.

Cloud water Cl^- concentrations and CAS number concentration data for diameters above 5 μm in the first ~100 m above sea level, termed CAS_{SF} hereafter (SF = near surface), are used as chemical and size distribution proxies for GCCN, respectively. These two are chosen for the following reasons. In terms of size distribution data, measurements from CPC and PCASP are limited due to their lower cutoff diameters being smaller than 1 μm, and while PCASP can be integrated above 1 μm, its upper size bound is only ~2.6 μm. *Colon-Robles et al.* [2006] showed that number concentration measurements from a cloud drop distribution probe exhibited improved correlations with surface wind speed as compared to the CPC or PCASP; they concluded that the former is better suited for GCCN quantification. To decide how best to calculate CAS_{SF}, different minimum threshold diameters were compared (2 μm, 3 μm, and 5 μm) and the results when using 5 μm revealed a higher correlation between CAS_{SF} and surface wind speed (termed $Wind_{SF}$ hereafter). In addition, the exponent in the power law regression, $CAS_{SF} = a \times Wind_{SF}^{b}$, was 1.0 when using a threshold diameter of 5 μm in contrast to having used smaller diameters.

Chloride is chosen as the GCCN chemical tracer as it is a major component of sea salt and more data are available in our data set as compared to the other major sea salt component, Na. The following two findings support the use of cloud water Cl^- as a chemical proxy for sea salt in our data set: (i) CAS_{SF} was best correlated with cloud water Cl^- (followed by Na) out of over 60 water-soluble ions and elements measured by IC and ICP-MS and (ii) the average (±1 standard deviation) of the Cl^-:Na mass ratio from E-PEACE and NiCE samples is 1.75 ± 0.58, which is close to that of natural sea salt (1.8).

It is important to address limitations associated with the two proxies introduced above. While CAS_{SF} is intended to represent GCCN at cloud base level, it had to be measured below cloud base altitude to avoid interference with fog and cloud droplets that could be encountered on aircraft level legs near cloud base. To assess the extent to which CAS_{SF} is related to GCCN near cloud base, Figures 2a and 2b compare CAS_{SF} concentrations to subcloud PCASP number concentrations integrated above both 0.1 μm and 1 μm (i.e., $PCASP_{Dp > 1\mu m}$), the latter of which is representative of GCCN between diameters of 1 and 2.6 μm. A power law regression ($y = a \times x^b$) reveals that in contrast to total PCASP concentration (≥0.1 μm), $PCASP_{Dp > 1\ \mu m}$ is at least positively related to CAS_{SF} ($r = 0.34$, $n = 76$). When removing one point with the lowest CAS_{SF} value in the latter plot (Figure 2b), the correlation improves ($r = 0.40$).

Thus, there is support for CAS_{SF} being related to GCCN near cloud base, although the relationship is not very strong owing to interferences such as the challenge of transporting GCCN to cloud base. Other limitations of CAS_{SF} considered here to be insignificant include the fact that the altitude and ambient RH coincident with each CAS_{SF} measurement will vary. The average (± standard deviation) of altitude and RH for the CAS_{SF} data used are 67 ± 25 m and 91 ± 5%, respectively. While the majority of CAS_{SF} data are from below 100 m, it is noted that 5 out of 100 points reached higher altitudes with a maximum of 155 m.

To address the issue of submicrometer sea salt particles [e.g., *O'Dowd and De Leeuw*, 2007] interfering with the use of Cl^- as a proxy for giant salt particles, mass concentrations of cloud water NaCl were used to back calculate the number concentration of particles needed to reach that exact mass concentration using the density of NaCl (2.2 g cm^{-3}) and the assumption of spherical particles. If the calculated concentration exceeds the measured value, this would indicate that submicrometer salt particles cannot account for the measured cloud water NaCl levels. The assumption of sphericity is reasonable, as the average surface relative humidity (RH) in the data set (90.3 ± 10.6%) exceeds the deliquescence RH of NaCl (75%). Note that the hygroscopic growth factor of NaCl around 90% RH is ~2.3 for a 200 nm particle [*Sorooshian et al.,* 2008]. The concentration of NaCl was computed in two ways: (i) as the sum of Cl^- and Na and (ii) as the sum of measured Cl^- and a derived Na^+ value from the Cl:Na ratio for natural sea salt (1.8). Both methods yielded similar results, and thus, we use the latter approach here. The ratio of calculated versus measured subcloud PCASP number concentration was 40 ± 60; the calculated value assumed that there were only 0.1 μm diameter sea salt particles. The same ratio calculated with subcloud CPC concentrations (instead of PCASP) yields 20 ± 35. When assuming a sea salt particle diameter of 0.2 μm, which is close to the median diameter of PCASP data (0.23 μm ± 0.05 μm), the ratios are as follows: 5 ± 9 (PCASP) and 2 ± 4 (CPC). These values are lower limits, as these calculations assume that the sampled particles are composed only of sea salt, when in reality, NaCl may account for approximately half of the dissolved nonwater species mass concentrations in cloud water in the study region [*Wang et al.,* 2014]. The calculations reported here are supportive of the overwhelming influence of supermicrometer sea salt particles, and not submicrometer particles, in driving Na and Cl^- mass concentrations in the measured cloud water.

While cloud water Cl^- concentrations are driven by GCCN, this certainly does not preclude the ability of smaller particles to be transported with GCCN owing to wind-driven processes. Figures 2c and 2d show power law fits to data for cloud water Cl^- and total subcloud PCASP concentrations ($r = 0.43$) and also for subcloud $PCASP_{Dp > 1\ \mu m}$ and subcloud PCASP concentration for diameters below 1 μm ($PCASP_{Dp < 1\ \mu m}$) ($r = 0.24$), respectively. These correlation results are suggestive of simultaneous lofting of submicrometer and supermicrometer particles to cloud base altitudes. However, the supermicrometer particles contribute to the majority of the Cl^- mass in cloud water, which is reinforced by the fact that 83.5 ± 8.3% of PCASP volume concentrations resides above 1 μm.

Since Figure 2 provides support for the relationship between CAS_{SF} and subcloud GCCN and that between GCCN and water Cl^-, it is expected that CAS_{SF} and Cl^- should exhibit a significant correlation with one another. This is indeed the case, since Cl^- is significantly correlated with CAS_{SF} (Figure 3a; $r = 0.49$, $n = 50$) based on a two-tailed t test with 95% confidence (hereafter, statistical significance coincides with the aforementioned requirement). In addition, CAS_{SF} and Cl^- both exhibit statistically significant correlations with $Wind_{SF}$ using a power law fit with r values of 0.39 ($n = 33$) and 0.36 ($n = 88$), respectively (Figure 3b).

While our data set cannot provide unambiguous proof of giant salt particles in cloud, the evaluation of the two proxies described above provides confidence that the use of both CAS_{SF} and Cl^-, but especially Cl^-, can represent their presence. This is supported by the similarity of the Cl^-:Na ratio to natural sea salt, the significant correlation between CAS_{SF} and Cl^- (and intermediate step being $PCASP_{Dp>1\mu m}$), and overall calculations indicating that it is impossible that submicrometer aerosol can account for the NaCl concentrations measured in cloud water.

3.2. GCCN Proxy Variable Interrelationships

Here we examine variables that influence the relationship between CAS_{SF} and Cl^-. To determine those factors in our data set that are most influential, a two-parameter power law regression analysis ($Cl^- \sim a \times CAS_{SF}^{\alpha} Y^{\beta}$) was conducted to identify those variables that most improve prediction capability as quantified by the model correlation coefficient.

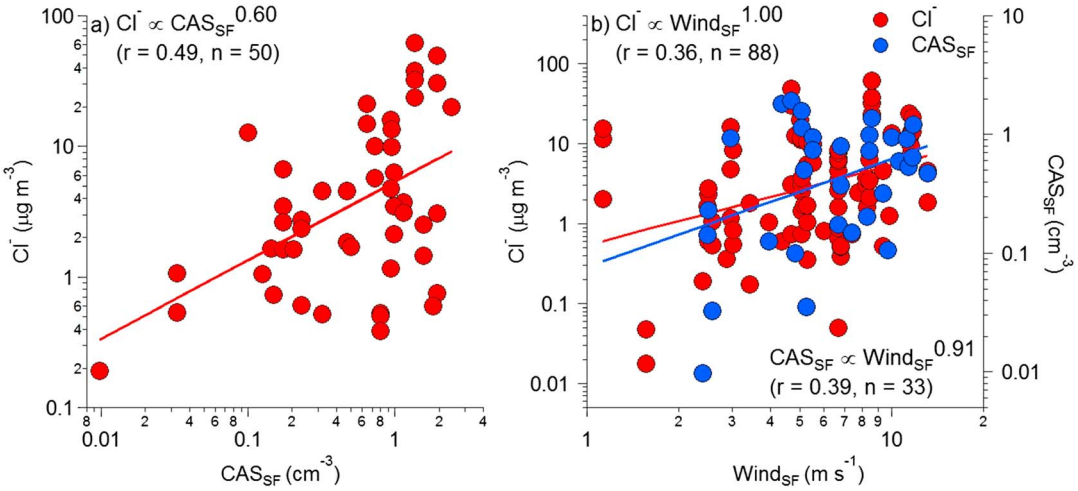

Figure 3. Relationship between (a) cloud water Cl^- and CAS_{SF} and (b) cloud water Cl^-, CAS_{SF}, and $Wind_{SF}$. These results are based on data from the E-PEACE and NiCE campaigns.

Among the strongest predictors are mean columnar rain rate (R) and subcloud standard deviation of the vertical velocity (σ_w). Figures 4 and 5 compare Cl^- and CAS_{SF} as a function of R and σ_w, respectively. More specifically, Cl^- and CAS_{SF} data were divided into two bins of these latter variables with the threshold value being similar to the median values to yield similar numbers of data points for comparison ($R = 0.6$ mm d^{-1}; $\sigma_w = 0.25$ m s^{-1}). The relationship between Cl^- and CAS_{SF} significantly improves when $R < 0.6$ mm d^{-1} with the correlation (r) being 0.89 versus 0.33 for higher R values. Higher R values are coincident with more wet scavenging, and it is likely that Cl^--enriched drops in clouds are scavenged more effectively than GCCN below cloud bases near the surface (i.e., CAS_{SF}). This becomes more evident by comparing the average (± standard deviation) values of Cl^- and CAS_{SF} coinciding with the two panels of Figure 4: $Cl^- = 13.71 \pm 19.01$ μg m^{-3} and $CAS_{SF} = 0.53 \pm 0.56$ cm^{-3} for low R and $Cl^- = 5.58 \pm 8.71$ μg m^{-3} and $CAS_{SF} = 1.07 \pm 0.51$ cm^{-3} for high R.

The Cl^--CAS_{SF} relationship improves significantly when $\sigma_w > 0.25$ m s^{-1} as compared to lower values (Figure 5). The correlation (r) is 0.82 for $\sigma_w > 0.25$ m s^{-1} versus only 0.19 for $\sigma_w < 0.25$ m s^{-1}. Higher σ_w values coincide potentially with improved transport of GCCN to cloud bases, and this would be expected to result in higher average ratios of Cl^-:CAS_{SF}, which is the case: 8.4 ± 9.1 for low σ_w; 23.1 ± 26.4 for high σ_w. Although not shown, the Cl^--CAS_{SF} relationship also improves significantly when replacing σ_w with the average of only positive values of the subcloud vertical velocity.

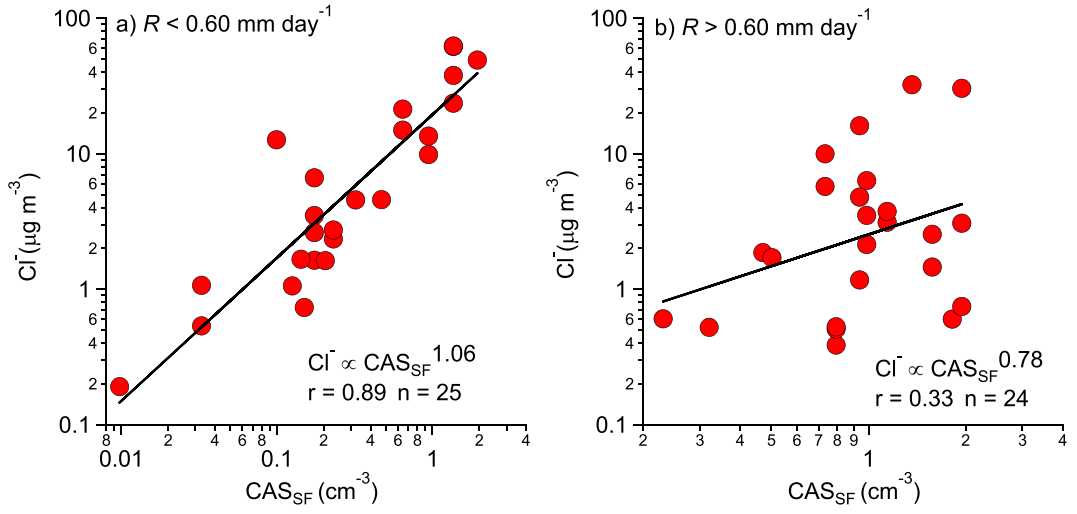

Figure 4. Relationship between cloud water Cl^- and CAS_{SF} for rain rates (a) < 0.60 mm d^{-1} and (b) > 0.60 mm d^{-1}. These results are based on data from the E-PEACE and NiCE campaigns.

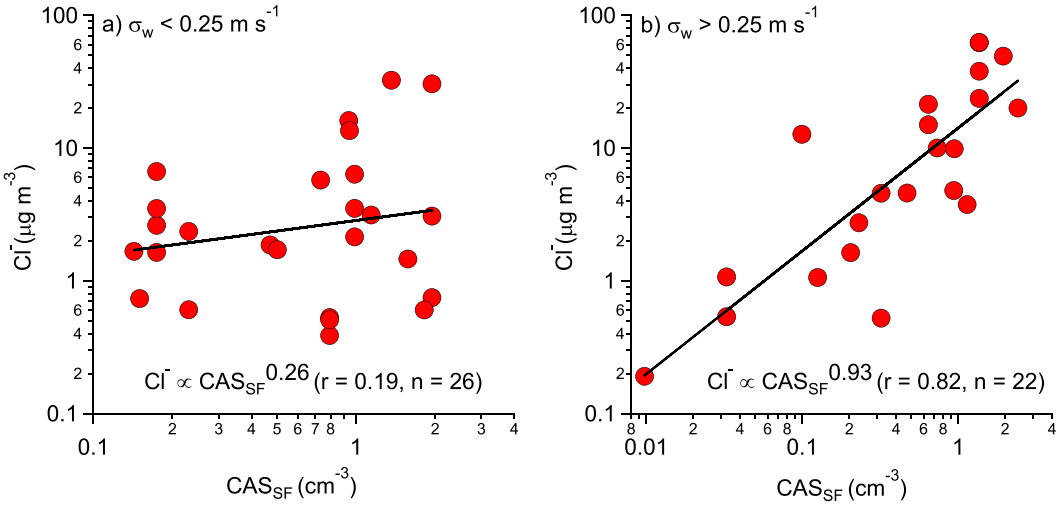

Figure 5. Relationship between cloud water Cl^- and CAS_{SF} for values of the subcloud vertical velocity standard deviation (σ_w) that are either (a) < 0.25 m s^{-1} or (b) > 0.25 m s^{-1}. These results are based on data from the E-PEACE and NiCE campaigns.

Figure 6 summarizes findings related to the Cl^--CAS_{SF} relationship with consideration of R and σ_w. When filtering occurs with these parameters to potentially reduce the influence of stronger wet scavenging (i.e., higher R) and weaker vertical transport (i.e., lower σ_w), the relationship improves ($r = 0.91$, $n = 18$) with a power law exponent close to unity (0.99) as compared to considering all points ($r = 0.49$, power law exponent = 0.60, $n = 50$).

3.3. Relationship Between GCCN and Cloud Properties

This section extends the use of the two GCCN proxy measurements to evaluate relationships with cloud properties. In terms of documented GCCN effects on clouds, modeling studies have shown that the effect of GCCN on warm rain initiation is effective only under certain conditions. *Feingold et al.* [1999] showed using a variety of models that in the case of stratocumulus clouds, the GCCN effect is greatest under conditions of either high CCN and LWP or low CCN and LWP. Subsequent studies suggested similar ideas about how the effect of GCCN is most influential as the concentration of smaller CCN increases [*Yin et al.,* 2000; *Teller and Levin*, 2006; *Cheng et al.,* 2009; *Dagan et al.,* 2015]. But even in that case, *Teller and Levin* [2006] suggest that the enhancement in precipitation rate as a result of GCCN is small relative to the overall suppression of precipitation owing to the large concentration of CCN. *L'Ecuyer et al.* [2009] used satellite remote sensing data and a global transport model to conclude that marine clouds influenced by high sea salt concentrations undergo accelerated broadening of drop spectra, form larger raindrops, precipitate more frequently, and are less vertically developed. Below we examine the extent to which use of cloud water Cl^- as an in-cloud GCCN proxy reproduces these documented results.

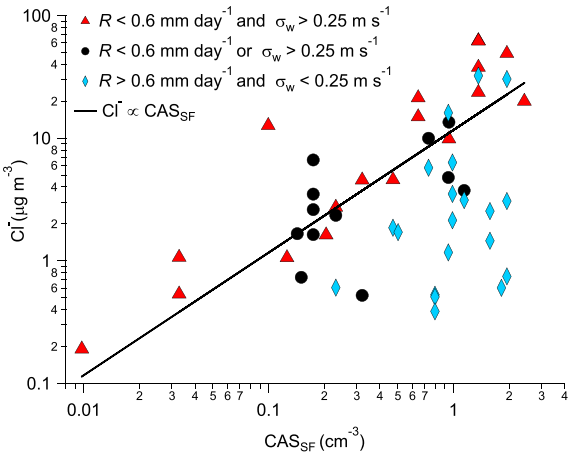

Figure 6. Relationship between cloud water Cl^- and CAS_{SF}, similar to Figure 3a, but with markers distinguishing between categories with different values of R and σ_w. The black markers correspond to data where only one of the two stated conditions are met, but not both. These results are based on data from the E-PEACE and NiCE campaigns.

3.3.1. Effects on Metric Values

A strategy employed to investigate the influence of aerosol particles on cloud characteristics involves quantification of physically relevant metrics such as the following:

$$\mathrm{ACI}_{r_e} = -\frac{d\ln(r_e)}{d\ln(N_d)} \quad (1)$$

$$\chi_{r_e} = \frac{d\ln(R)}{d\ln(r_e)} \quad (2)$$

Table 1. S_o, χ_{r_e}, ACI_{r_e}, and Relevant Parameters for Three Different Cloud Liquid Water Path Bins for Low (<3.0 μg m^{-3}) and High (>3.0 μg m^{-3}) Cloud Water Cl^- Concentrations[a]

	LWP (g m^{-2})	S_o	χ_{re}	ACI_{re}	r_e (μm)	R (mm d^{-1})	N_d (cm^{-3})	Cl^- (μg m^{-3})	CAS_{SF} (cm^{-3})
Low Cl^-	46 ± 21	**1.56 (0.73,22)**	**4.78 (0.93,22)**	**0.37 (0.90,22)**	9.09 ± 2.26	0.75 ± 0.88	130 ± 66	1.1 ± 0.7	0.56 ± 0.61
	104 ± 13	**0.46 (0.44,22)**	**2.03 (0.57,22)**	**0.27 (0.92,22)**	9.78 ± 2.22	0.93 ± 0.76	146 ± 68	1.3 ± 0.8	0.42 ± 0.53
	211 ± 80	**1.05 (0.76,21)**	**3.63 (0.83,21)**	**0.29 (0.93,21)**	11.75 ± 2.22	1.11 ± 0.84	99 ± 53	1.1 ± 0.9	0.56 ± 0.60
High Cl^-	49 ± 19	**1.52 (0.69,21)**	**3.99 (0.84,21)**	**0.44 (0.95,21)**	7.70 ± 1.45	0.44 ± 0.33	236 ± 84	11.8 ± 5.8	0.75 ± 0.16
	93 ± 11	0.54 (0.37,21)	**2.77 (0.54,21)**	**0.28 (0.96,21)**	8.89 ± 1.26	0.73 ± 0.40	181 ± 88	8.5 ± 7.7	0.73 ± 0.39
	174 ± 39	−0.28 (0.15,21)	0.58 (0.11,21)	**0.31 (0.82,21)**	9.41 ± 0.88	0.50 ± 0.23	180 ± 48	21.2 ± 20.0	1.17 ± 0.66

[a]Values in parentheses: (correlation coefficient *r*, sample size). Correlations that are statically significant based on a two-tailed *t* test with 95% confidence have been marked with bold font. These results are based on data from the E-PEACE and NiCE campaigns.

$$S_o = -\frac{d\ln(R)}{d\ln(N_d)}. \quad (3)$$

The ACI_{r_e} metric quantifies the response of a cloud microphysical parameter (r_e) to an aerosol perturbation (with drop concentration, N_d, as the aerosol proxy here). The relationship between aerosol perturbations and R can be quantified using the precipitation susceptibility (S_o) term, which relates precipitation rate responses to changes in N_d. S_o can be indirectly obtained by the product of ACI_{r_e} and χ_{r_e}, the latter of which quantifies the response of R to changes in r_e [*Sorooshian et al.,* 2010]. All three metrics are typically evaluated in bins of a cloud macrophysical property, which is usually LWP (chosen here) or cloud depth.

Numerous studies have examined how S_o depends on LWP [e.g., *Lu et al.,* 2009; *Wood et al.,* 2009; *Sorooshian et al.,* 2009, 2010; *Jiang et al.,* 2010; *Bangert et al.,* 2011; *Duong et al.,* 2011; *Gettelman et al.,* 2013; *Mann et al.,* 2014] and cloud thickness [*Terai et al.,* 2012; *Jung et al.,* 2016]. Some studies report that S_o typically increases up to a specific LWP at which point it drops in value reflecting a switch from a dominant autoconversion process to an accretion process. The other subset of studies, focused mainly on stratocumulus clouds, reports a general reduction in S_o as a function of LWP or cloud thickness. Differences in these studies include (but are not limited to) differences in the following: (i) cloud type [*Lebo and Feingold*, 2014], (ii) choices of how to calculate parameters included in quantifying S_o [*Duong et al.,* 2011], (iii) minimum threshold value for rain rate [*Duong et al.,* 2011], (iv) lower tropospheric static stability [*Sorooshian et al.,* 2009], and (v) "cloud contact time," defined as the time an air parcel spends in cloud [*Feingold et al.,* 2013].

Table 1 summarizes results for the three metrics in equations 1–3 for two different bins of Cl^- divided at 3.0 μg m^{-3} to maintain similar data point numbers (n = 65 and 63 for low and high Cl^-, respectively). As expected from previous discussion, CAS_{SF} is higher in the high Cl^- category. N_d is also enhanced in the latter category owing to more submicrometer particles being lofted up to cloud base, resulting in lower r_e and suppressed R. This is consistent with the results of others showing that an enhancement of GCCN does not necessarily lead to enhanced R owing to the suppression of R due to a greater number of smaller CCN [e.g., *Teller and Levin*, 2006].

The metric values are reported in three LWP bins with similar data point numbers. As expected, ACI_{re} is, on average, close to 1/3 for the three LWP bins shown in Table 1. For low Cl^- clouds, S_o decreases from 1.56 in the lowest LWP bin to 0.46 before increasing again to 1.05 in the highest LWP bin. The trend in χ_{r_e} values mimics that of S_o as a function of LWP, as has been shown before [*Sorooshian et al.,* 2010]. For high Cl^- clouds, S_o decreases continuously from 1.52 to −0.28 for the three LWP bins. Again, it is shown that χ_{r_e} follows the same LWP-dependent trend as S_o. It is noted that of all metric values in Table 1, the only three that were not statistically significant at 95% confidence were for S_o in the intermediate LWP bin and S_o and χ_{r_e} at the highest LWP bin for high Cl^- clouds. It is this last LWP bin that reveals the key difference between the two Cl^- categories, with more GCCN (as inferred by higher Cl^-) leading to a negative S_o value. The low statistical significance of that point could be due to multiple competing effects such as with suppression of rain with more particles and enhancement of rain owing to GCCN. Another study showed that marine stratocumulus clouds can sometimes exhibit negative S_o values and attributed it to factors such as turbulence, GCCN, or satellite retrieval artifacts [*Terai et al.,* 2015]. Our results support the idea that GCCN could potentially be responsible for the counterintuitive negative S_o values.

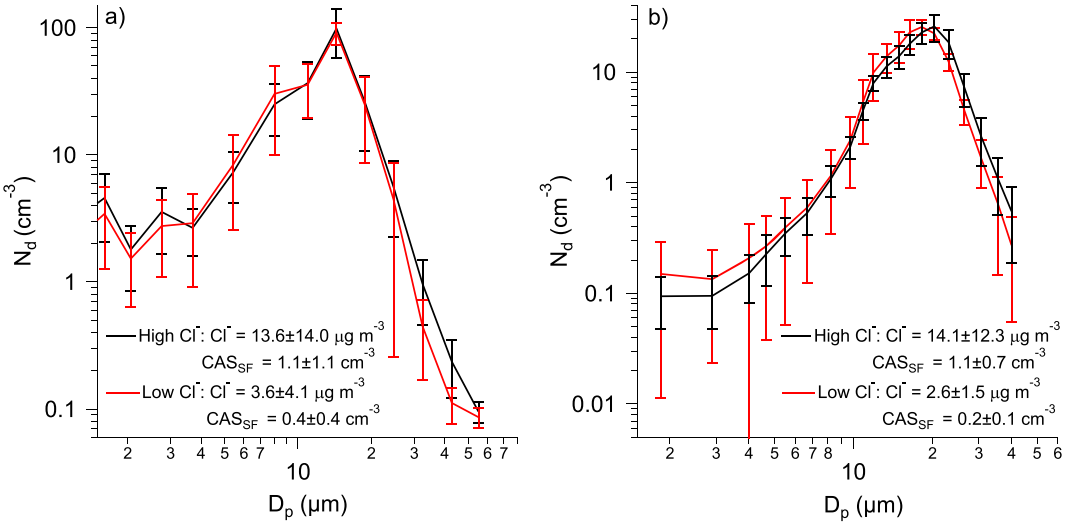

Figure 7. Comparison of drop size distributions between conditions of high and low cloud water Cl^- during (a) E-PEACE and (b) NiCE. Average Cl^- concentrations and CAS_{SF} values for each category are reported in the inset legends to demonstrate in two ways the significant difference in GCCN. Whiskers represent one standard deviation.

3.3.2. Effects on Drop Distribution

As the effects of GCCN on clouds are driven largely by changes in the cloud drop distribution, Figure 7 contrasts mean columnar drop spectra for cases of high and low cloud water Cl^- concentrations during E-PEACE and NiCE. A total of 12 pairs of cases are examined, with each set having data from a flight with low Cl^- and another flight with high Cl^- (Table 2). The pairs were chosen such that the two cases being

Table 2. Summary of Parameters Relevant to the 12 Pairs of Cases Comparing High and Low Cloud Water Cl^- Concentrations for Clouds With Similar LWP and N_d Values[a]

Pair #	Date	RF	Cl^- (μg m^{-3})	CAS_{SF} (cm^{-3})	r_e (μm)	R (mm d^{-1})	LWP (g m^{-2})	N_d (cm^{-3})	PCASP (cm^{-3})	σ_w (m s^{-1})
1	25 Jul 2013	14	7.7	NA	**9.85**	**0.47**	219	161	188	0.18
	25 Jul 2013	14	0.9	NA	**8.91**	**0.26**	214	166	NA	0.32
2	29 Jul 2013	16	32.3	1.36	**10.86**	**0.81**	176	156	**392**	0.23
	25 Jul 2013	14	4.6	NA	**9.24**	**0.25**	176	159	**277**	0.27
3	16 Jul 2013	7	5.5	0.44	10.43	**0.69**	167	124	240	0.30
	22 Jul 2013	11	2.3	0.23	10.12	**0.37**	160	124	231	0.17
4	29 Jul 2013	16	10.9	**1.36**	9.45	**0.43**	95	131	**181**	0.31
	9 Jul 2013	2	2.6	**0.17**	9.04	**0.18**	97	134	**203**	0.11
5	9 Jul 2011	2	11.4	NA	**7.81**	**0.68**	121	**283**	NA	0.23
	2 Aug 2011	18	0.5	**0.03**	**7.51**	**0.40**	119	**242**	325	0.38
6	23 Jul 2011	11	16.1	**0.94**	**9.29**	**1.35**	97	159	**287**	0.21
	10 Aug 2011	24	10.0	**0.73**	**8.56**	**0.76**	92	162	**432**	0.24
7	10 Aug 2011	24	5.7	**0.73**	9.29	**0.95**	59	127	157	0.21
	16 Aug 2011	28	0.6	**1.82**	9.31	**0.51**	54	126	NA	NA
8	9 Aug 2011	23	9.9	**0.94**	**7.20**	**0.26**	45	**252**	352	0.41
	24 Jul 2011	12	1.7	**0.14**	**6.47**	**0.13**	44	**237**	NA	NA
9	22 Jul 2011	10	3.1	**1.14**	9.81	0.81	80	125	210	0.24
	11 Aug 2011	25	0.4	**0.79**	9.80	0.77	82	124	231	0.19
10	10 Aug 2011	24	10.0	**0.73**	**8.73**	**0.55**	73	160	268	0.32
	27 Jul 2011	14	1.7	**0.50**	**8.13**	**0.37**	71	162	NA	NA
11	8 Aug 2011	22	14.3	0.64	**7.46**	0.38	59	297	**449**	0.28
	12 Aug 2011	26	7.4	0.71	**6.92**	0.36	69	306	**566**	0.36
12	8 Jul 2011	1	20.0	**2.42**	**7.28**	NA	29	**231**	304	0.30
	1 Aug 2011	17	0.2	**0.01**	**6.64**	0.10	33	**219**	292	0.29

[a]Parameter values that could not be calculated robustly due to instrument issues or insufficient time for collect sufficient data are denoted with "NA, not applicable." Values (except for Cl^- and σ_w) that exhibit statistically significant differences in each pair have been marked with bold font. These results are based on data from the E-PEACE and NiCE campaigns, with the given research flight provided under the "RF" column.

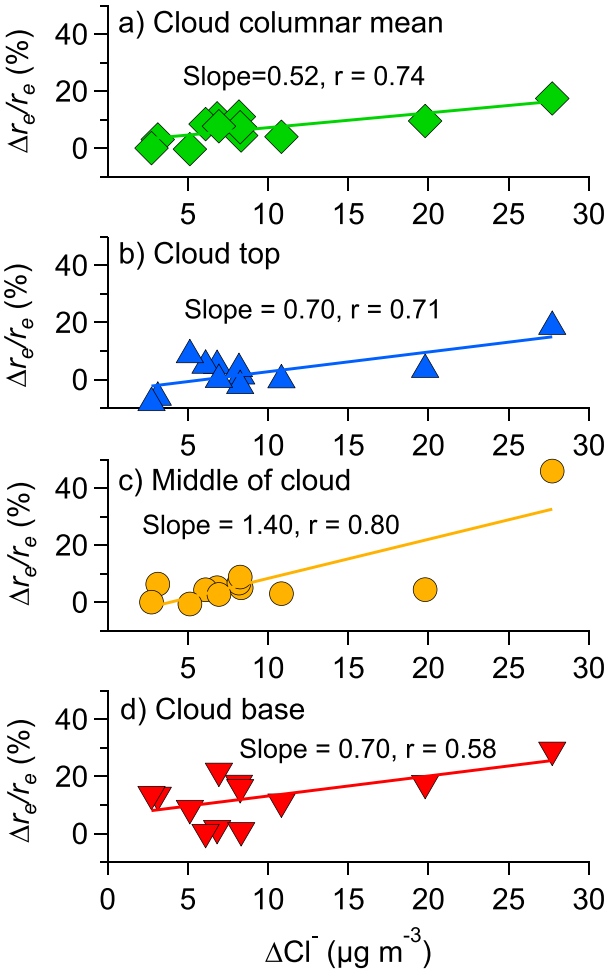

Figure 8. Relationship between $\Delta r_e/r_e$ versus ΔCl^- for the 12 pairs of cases in Table 2 for different regions of clouds: vertically averaged over (a) the full cloud depth, (b) the top third ("cloud top"), (c) middle third ("middle of cloud"), and (d) the bottom third ("cloud base"). These results are based on data from the E-PEACE and NiCE campaigns.

compared are characterized by having similar LWP and N_d values to remove the influence of meteorology and submicrometer particle concentration, respectively, on cloud properties. It is noted that the number of data points used to calculate the values in Table 2 varies between the cases. Values of LWP and N_d are within 10% between cases for most pairs (Table 2); the exceptions include pairs 11 and 12, where differences of LWP are ~15%, and pair 5 where N_d differs by ~15%. The high Cl^- cases in E-PEACE and NiCE exhibited Cl^- and CAS_{SF} concentrations that were ~3–6 times larger than the respective low Cl^- cases. The drop spectra reveal that drop concentrations are higher above 20 μm in the high Cl^- category, with the greatest enhancements above 30 μm. Past work has suggested that cloud top r_e values around 12–14 μm mark the initiation of rain [*Rosenfeld et al.,* 2012], which is coincident with the sizes where the drop concentrations are enhanced under high GCCN conditions in the current study. It is cautioned that the ability of GCCN to form large drops in clouds can be offset by strong updraft velocities, which can increase the peak supersaturation leading to more numerous but smaller drops [*Colon-Robles et al.,* 2006]. To address this competitive effect, we determined that σ_w is not always higher for the high Cl^- cases (Table 2). For the nine pairs where σ_w values could be calculated, five were characterized by having higher σ_w values in the low Cl^- case.

3.3.3. Effects on Drop Effective Radius and Precipitation

Figures 8a–8d show how changes in Cl^- concentration (ΔCl^-) between the two cases among each of the 12 pairs in Table 2 relate to $\Delta r_e/r_e$, where the denominator is the r_e value in the low Cl^- case, which is hereafter referred to as the baseline case. The relationship is shown for the bottom (i.e., base), middle, and top third of clouds, in addition to the entire cloud column. Regardless of vertical location in cloud, $\Delta r_e/r_e$ is shown to increase as a function of ΔCl^- with statistical significance ($r = 0.58$–0.80). This result is consistent with past work showing that the effect of GCCN enhancing drop size may be larger in more polluted conditions and in clouds not drizzling heavily already since lower r_e is typically observed with more drops at fixed LWP [e.g., *Cheng et al.,* 2009].

A key feature in Figures 8b–8d is how the value of $\Delta r_e/r_e$ decreases as a function of height in cloud, suggestive of how GCCN-produced raindrops precipitate before reaching the top portions of clouds. The average value of $\Delta r_e/r_e$ for the three vertical bins of clouds is as follows: base = 12.8% ± 8.8%, "middle" = 7.7% ± 12.3%, and "top" = 2.4% ± 7.0%. Figure 9 illustrates the difference between the percentage increase of r_e between the bottom and top third of clouds as a function of Cl^- for all cases in Table 2; note that this relaxes the

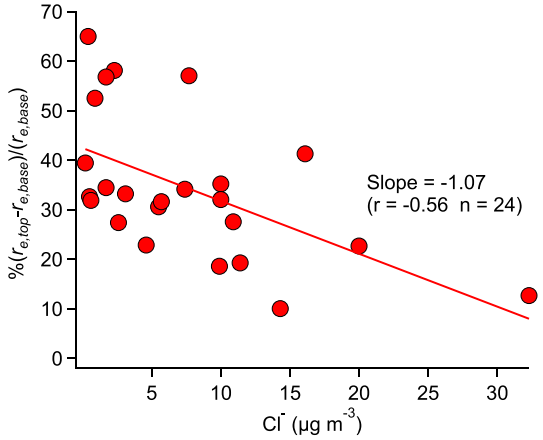

Figure 9. Relationship between the percent change in r_e from the bottom third to the top third of clouds as a function of Cl^- for the 24 cases in Table 2. These results are based on data from the E-PEACE and NiCE campaigns.

requirement of comparing cases with similar N_d and LWP. A significant negative correlation ($r = -0.56$) is evident, showing in another way how GCCN can affect the vertical microphysical structure of clouds.

Figure 10 shows an analogous analysis compared to Figure 8a except with r_e replaced by R. A positive relationship is observed in Figure 10, which is assisted greatly by the highest ΔCl^- data point. When that point is omitted from the analysis, the positive relationship is preserved but it is not statistically significant ($r = 0.30$). This is indicative of a more complex relationship between GCCN and R as compared to r_e since the latter parameter is more closely connected to aerosol particles in the chain of events leading from an aerosol perturbation to a precipitation response. Although there are limited data points, the combination of Figures 8 and 10 suggests that increases in cloud water Cl^- are coincident with larger enhancements in r_e and R, with the relationship being more pronounced for more polluted conditions and less precipitating clouds. Further validation from other experimental data sets is encouraged.

4. GCCN Effects on Precipitation in Modern Era Retrospective Analysis for Research and Applications Version 2

There are at least two ways to address the issue of limited data points. One is through future field campaigns and the other is through modern data assimilation. The latter does not involve the direct measurement of the relevant quantities, but it increases the number of data points by several orders of magnitude. Here we analyze aerosol particles, clouds, and precipitation in the Modern Era Retrospective Analysis for Research and Applications version 2 (MERRA-2) as an attempt in this direction. Recognizing the difference between limited aircraft measurements along flight legs versus a large number of grid box averages from a reanalysis, we are not using one to validate another. Rather, we hope to check if the direction of change is consistent.

MERRA-2 utilizes the Goddard Earth Observing System version 5 (GEOS-5) atmospheric general circulation model that includes modifications to the moist physics, turbulent, surface, and gravity wave drag parameterizations [*Molod et al.,* 2015]. Large-scale condensation is derived from a "top-hat"-shaped probability density function as in *Bacmeister et al.* [2006]. Autoconversion and accretion are parameterized using Sundqvist-like formulations, and precipitation is assumed to completely fall out [*Rienecker et al.,* 2008]. Unlike in MERRA, an aerosol model [*Chin et al.,* 2002] is also used to actively simulate the generation, removal, and transport of aerosol particles rather than including prescribed particles. Thus, there are several data collections that include various measures of aerosol content in MERRA-2 [*Bosilovich et al.,* 2016]. Of these, we utilize the instantaneous 3 h sea salt mixing ratios from the lowest model layer (corresponding to pressures ≥ 985 hPa) to derive instantaneous sea salt mass concentrations. We define the giant sea salt concentration (GSSC) as the

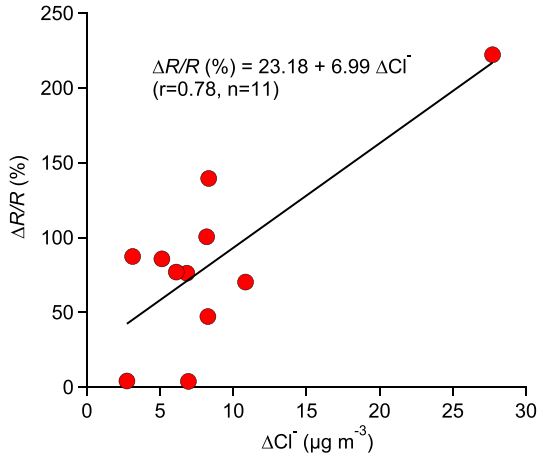

Figure 10. Relationship between $\Delta R/R$ from vertically averaged rain rate versus ΔCl^- for the 12 pairs of cases in Table 2. These results are based on data from the E-PEACE and NiCE campaigns.

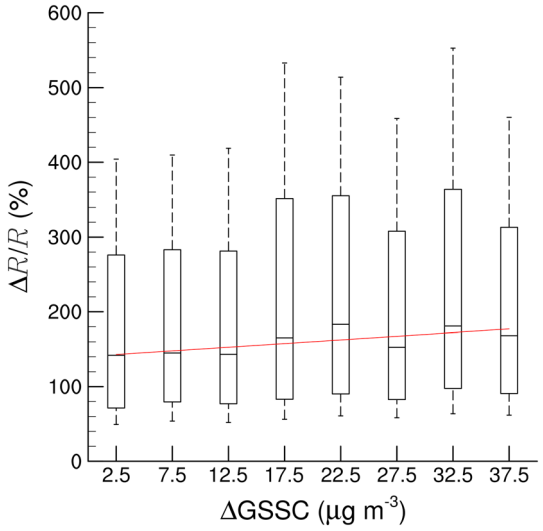

Figure 11. MERRA-2 reanalysis data analysis showing how $\Delta R/R$ responds to varying levels of change in giant sea salt mass concentration (ΔGSSC) for 40 completely ocean grid cells within the region bounded by 34°N–40°N and 121.5°W–125°W during July of 2005, 2007, 2011, and 2013. Comparison pairs are for 18 Z only in which low clouds (at pressures ≥ 750 hPa) and surface precipitation are present at both times. Also, surface precipitation has to be less at the time that GSSC was lower. The top and bottom of the boxes are the upper and lower terciles of bins 5 μg m^{-3} wide in ΔGSSC, while the whiskers indicate the upper and lower quartiles. The horizontal lines inside of the boxes are the bin medians. The linear regression of the bin medians is also given as the red line.

sum of those from bins 4 and 5 for particles with dry radii of 1.5–5 and 5–10 μm, respectively, to coincide as closely as possible to the GCCN cutoff diameter of 5 μm defined for the aircraft data. Surface precipitation and LWP are provided as hourly averages, so we compare the averages of these for the two hours before and after the times of the instantaneous GSSCs.

For the 12 observation pairs compared in Table 2, we have compared the GSSCs at the closest instantaneous 3 h values for the grid cell containing the observations. For all but the first pair, MERRA-2 has higher GSSC for instances of greater observed Cl^-. However, the modeled weather conditions may not necessarily correspond to those observed, as not all of these instances have clouds or surface precipitation. Therefore, to evaluate MERRA-2 data for similar weather conditions as observed during the aircraft campaigns, we extend our analysis to complete ocean grid cells between 34°N and 40°N and 121.5°W and 125°W (Figure 1) for all of July in the years in which flight campaigns took place (2005, 2007, 2011, and 2013). This includes 40 grid cells for 1240 3-hourly instances. Of these, we pick comparison pairs at 18 Z only; this corresponds roughly with the same time of the observations from Table 2. For comparisons for similar weather conditions to those observed during the research flights, we limit our comparisons to instances of low clouds (at pressures ≥750 hPa) that have surface precipitation at both times. This gives us a total of 33,812 pairs for comparison.

Figure 11 shows the variation in the relative change of MERRA-2 surface precipitation ($\Delta R/R$) as a function of ΔGSSC for 16,272 pairs when the sign in the difference in surface precipitation matches that of the GSSC. The spread in $\Delta R/R$ is quite large, but the general trend is upward with increasing ΔGSSC as indicated by the linear regression of the bin medians (red line). The trend is consistent in sign with the aircraft data, but much weaker in MERRA-2 than for observed ΔCl^- as evident by comparing the following slopes: $\Delta R/R$ versus ΔGSSC: 0.97/μg m^{-3} ΔGSSC as opposed to 6.99/μg m^{-3} ΔCl^-. Part of this difference might be due to the physical difference in GSSC and Cl^-, but most of this is likely due to inadequacies in the parameterization of cloud and precipitation microphysics.

For the other 17,540 pairs when the difference in surface precipitation is opposite that of GSSC, there is a poorer relationship between precipitation and GSSC. For these, dynamics seems to be more important to precipitation, being higher when the surface pressure is lower (not shown), presumably when above-cloud subsidence would be lower. This suggests that GCCN only slightly enhances the effect of large-scale dynamics on cloud processes in MERRA-2 when GSSC is higher and subsidence is lower.

5. Conclusions

This work uses airborne data to address the challenge of identifying the presence of GCCN and quantifying their effects on clouds. The analyses presented explores the use of cloud water Cl^- concentration and near-surface particle number concentration with $D_p > 5$ μm as proxies for GCCN in the marine atmosphere. The two variables are shown to be consistent with the relationships expected of sea salt and factors driving its emission to the atmosphere and subsequent effects. The interrelationship between the two parameters is influenced by precipitation rate, owing to wet scavenging effects, and the standard deviations of the

subcloud vertical velocity. The difference in r_e between high and low Cl^- decreases with height in cloud, suggesting that some GCCN-produced raindrops precipitate before reaching cloud tops.

Aircraft data are limited in their spatiotemporal coverage and statistics. To address this issue, reanalysis data (MERRA-2) were examined as the number of data points available are orders of magnitude larger than those from aircraft. The sign of the cloud responses (i.e., surface precipitation rate) to perturbations in GSSC was similar between MERRA-2 and the aircraft data. The magnitude of the responses was stronger in the aircraft data set, which likely is due to fewer data points, the physical difference between GSSC and Cl^-, and inadequacies in the parameterization of cloud and precipitation microphysics. Future work is encouraged to continue using proxy measurements for GCCN to evaluate archived and future field data sets with the goal of improving model parameterizations of aerosol-cloud relationships.

Acknowledgments
All data and results are available from the corresponding author (armin@email.arizona.edu). This work was funded by NASA grant NNX14AM02G and Office of Naval Research grants N00014-10-1-0811, N00014-11-1-0783, N00014-10-1-0200, N00014-04-1-0118, and N00014-16-1-2567. We acknowledge Daniel Rosenfeld and two anonymous reviewers for helpful comments.

References

Bacmeister, J. T., M. J. Suarez, and F. R. Robertson (2006), Rain reevaporation, boundary layer convection interactions, and Pacific rainfall patterns in a AGCM, *J. Atmos. Sci.*, *63*, 3383–3403.

Bangert, M., C. Kottmeier, B. Vogel, and H. Vogel (2011), Regional scale effects of the aerosol cloud interaction simulated with an online coupled comprehensive chemistry model, *Atmos. Chem. Phys.*, *11*(9), 4411–4423.

Bosilovich, M. G., R. Lucchesi, and M. Suarez (2016), MERRA-2: File specification. GMAO Office Note No. 9 (Version 1.1), 73 pp. [Available at http://gmao.gsfc.nasa.gov/pubs/office_notes.]

Chen, Y. C., M. W. Christensen, L. Xue, A. Sorooshian, G. L. Stephens, R. M. Rasmussen, and J. H. Seinfeld (2012), Occurrence of lower cloud albedo in ship tracks, *Atmos. Chem. Phys.*, *12*(17), 8223–8235.

Cheng, W. Y. Y., G. G. Carrio, W. R. Cotton, and S. M. Saleeby (2009), Influence of cloud condensation and giant cloud condensation nuclei on the development of precipitating trade wind cumuli in a large eddy simulation, *J. Geophys. Res.*, *114*, D08201, doi:10.1029/2008JD011011.

Chin, M., P. Ginoux, S. Kinne, B. N. Holben, B. N. Duncan, R. V. Martin, J. A. Logan, A. Higurashi, and T. Nakajima (2002), Tropospheric aerosol optical thickness from the GOCART model and comparisons with satellite and Sun photometer measurements, *J. Atmos. Sci.*, *59*, 461–483, doi:10.1175/1520-0469(2002)059<0461:TAOTFT>2.0.CO;2.

Coggon, M. M., A. Sorooshian, Z. Wang, J. S. Craven, A. R. Metcalf, J. J. Lin, A. Nenes, H. H. Jonsson, R. C. Flagan, and J. H. Seinfeld (2014), Observations of continental biogenic impacts on marine aerosol and clouds off the coast of California, *J. Geophys. Res. Atmos.*, *119*, 6724–6748, doi:10.1002/2013JD021228.

Colon-Robles, M., R. M. Rauber, and J. B. Jensen (2006), Influence of low-level wind speed on droplet spectra near cloud base in trade wind cumulus, *Geophys. Res. Lett.*, *33*, L20814, doi:10.1029/2006GL027487.

Crosbie, E., et al. (2016), Stratocumulus cloud clearings and notable thermodynamic and aerosol contrasts across the clear-cloudy interface, *J. Atmos. Sci.*, *73*(3), 1083–1099.

Dagan, G., I. Koren, and O. Altaratz (2015), Aerosol effects on the timing of warm rain processes, *Geophys. Res. Lett.*, *42*, 4590–4598, doi:10.1002/2015GL063839.

Duong, H. T., A. Sorooshian, and G. Feingold (2011), Investigating potential biases in observed and modeled metrics of aerosol-cloud-precipitation interactions, *Atmos. Chem. Phys.*, *11*(9), 4027–4037.

Feingold, G., W. R. Cotton, S. M. Kreidenweis, and J. T. Davis (1999), The impact of giant cloud condensation nuclei on drizzle formation in stratocumulus: Implications for cloud radiative properties, *J. Atmos. Sci.*, *56*(24), 4100–4117.

Feingold, G., A. McComiskey, D. Rosenfeld, and A. Sorooshian (2013), On the relationship between cloud contact time and precipitation susceptibility to aerosol, *J. Geophys. Res. Atmos.*, *118*, 10,544–10,554, doi:10.1002/jgrd.50819.

Gerber, H., B. G. Arends, and A. S. Ackerman (1994), New microphysics sensor for aircraft use, *Atmos. Res.*, *31*(4), 235–252.

Gettelman, A., H. Morrison, C. R. Terai, and R. Wood (2013), Microphysical process rates and global aerosol-cloud interactions, *Atmos. Chem. Phys.*, *13*(19), 9855–9867.

Hegg, D. A., and P. V. Hobbs (1986), Studies of the mechanisms and rate with which nitrogen species are incorporated into cloud water and precipitation, Second Annual Report on Project CAPA-21-80 to the Coordinating Research Council.

Houghton, H. H. (1938), Problems connected with the condensation and precipitation processes in the atmosphere, *Bull. Am. Meteorol. Soc.*, *19*, 152–159.

Jensen, J. B., and S. H. Lee (2008), Giant sea-salt aerosols and warm rain formation in marine stratocumulus, *J. Atmos. Sci.*, *65*(12), 3678–3694.

Jiang, H. L., G. Feingold, and A. Sorooshian (2010), Effect of aerosol on the susceptibility and efficiency of precipitation in warm trade cumulus clouds, *J. Atmos. Sci.*, *67*(11), 3525–3540.

Johnson, D. B. (1982), The role of giant and ultragiant aerosol particles in warm rain initiation, *J. Atmos. Sci.*, *39*, 448–460.

Johnson, D. B. (1993), The onset of effective coalescence growth in convective clouds, *Q. J. R. Meteorol. Soc.*, *119*, 925–933.

Jung, E., B. A. Albrecht, H. H. Jonsson, Y. C. Chen, J. H. Seinfeld, A. Sorooshian, A. R. Metcalf, S. Song, M. Fang, and L. M. Russell (2015), Precipitation effects of giant cloud condensation nuclei artificially introduced into stratocumulus clouds, *Atmos. Chem. Phys.*, *15*(10), 5645–5658.

Jung, E., B. A. Albrecht, A. Sorooshian, P. Zuidema, and H. H. Jonsson (2016), Precipitation susceptibility in marine stratocumulus and shallow cumulus from airborne measurements, *Atmos. Chem. Phys.*, *16*, 11,395–11,413, doi:10.5194/acp-16-11395-2016.

Knight, C. A., J. Vivekanandan, and S. G. Lasher-Trapp (2002), First radar echoes and the early ZDR history of Florida cumulus, *J. Atmos. Sci.*, *59*, 1454–1472.

Laird, N. F., H. T. Ochs III, R. M. Rauber, and L. J. Miller (2000), Initial precipitation formation in warm Florida cumulus, *J. Atmos. Sci.*, *57*, 3740–3751.

Lasher-Trapp, S. G., C. A. Knight, and J. M. Straka (2001), Early radar echoes from ultragiant aerosol in a cumulus congestus: Modeling and observations, *J. Atmos. Sci.*, *58*, 3545–3562.

Lebo, Z. J., and G. Feingold (2014), On the relationship between responses in cloud water and precipitation to changes in aerosol, *Atmos. Chem. Phys.*, *14*(21), 11,817–11,831, doi:10.5194/acp-14-11817-2014.

L'Ecuyer, T. S., W. Berg, J. Haynes, M. Lebsock, and T. Takemura (2009), Global observations of aerosol impacts on precipitation occurrence in warm maritime clouds, *J. Geophys. Res.*, *114*, D09211, doi:10.1029/2008JD011273.
Lewis, E. R., and S. E. Schwartz (Eds.) (2004), *Sea Salt Aerosol Production: Mechanisms, Methods, Measurements, and Models—A Critical Review, Geophys. Monogr. Ser*, vol. 152, AGU, Washington, D. C.
Lu, M. L., W. C. Conant, H. H. Jonsson, V. Varutbangkul, R. C. Flagan, and J. H. Seinfeld (2007), The Marine Stratus/Stratocumulus Experiment (MASE): Aerosol-cloud relationships in marine stratocumulus, *J. Geophys. Res.*, *112*, D10209, doi:10.1029/2006JD007985.
Lu, M. L., A. Sorooshian, H. H. Jonsson, G. Feingold, R. C. Flagan, and J. H. Seinfeld (2009), Marine stratocumulus aerosol-cloud relationships in the MASE-II experiment: Precipitation susceptibility in eastern Pacific marine stratocumulus, *J. Geophys. Res.*, *114*, D24203, doi:10.1029/2009JD012774.
Mann, J. A. L., J. C. Chiu, R. J. Hogan, E. J. O'Connor, T. S. L'Ecuyer, T. H. M. Stein, and A. Jefferson (2014), Aerosol impacts on drizzle properties in warm clouds from ARM Mobile Facility maritime and continental deployments, *J. Geophys. Res. Atmos.*, *119*, 4136–4148, doi:10.1002/2013JD021339.
Mason, B. J. (2001), The role of sea-salt particles as cloud condensation nuclei over the remote oceans, *Q. J. R. Meteorol. Soc.*, *127*(576), 2023–2032.
Mather, G. K. (1991), Coalescence enhancement in large multicell storms caused by the emissions from a Kraft Paper-Mill, *J. Appl. Meteorol.*, *30*(8), 1134–1146.
Maudlin, L. C., Z. Wang, H. H. Jonsson, and A. Sorooshian (2015), Impact of wildfires on size-resolved aerosol composition at a coastal California site, *Atmos. Environ.*, *119*, 59–68.
Modini, R. L., et al. (2015), Primary marine aerosol-cloud interactions off the coast of California, *J. Geophys. Res. Atmos.*, *120*, 4282–4303, doi:10.1002/2014JD022963.
Molod, A., L. Takacs, M. Suarez, and J. Bacmeister (2015), Development of the GEOS-5 atmospheric general circulation model: Evolution from MERRA to MERRA2, *Geosci. Model Dev.*, *8*, 1339–1356, doi:10.5194/gmd-8-1339-2015.
Ochs, H. T., and R. G. Semonin (1979), Sensitivity of a cloud microphysical model to an urban environment, *J. Appl. Meteorol.*, *18*, 1118–1129.
O'Dowd, C. D., and G. De Leeuw (2007), Marine aerosol production: A review of the current knowledge, *Philos. Trans. R. Soc. London, Ser. A*, *365*(1856), 1753–1774.
Prabhakar, G., B. Ervens, Z. Wang, L. C. Maudlin, M. M. Coggon, H. H. Jonsson, J. H. Seinfeld, and A. Sorooshian (2014), Sources of nitrate in stratocumulus cloud water: Airborne measurements during the 2011 E-PEACE and 2013 NiCE studies, *Atmos. Environ.*, *97*, 166–173.
Pruppacher, H. R., and J. D. Klett (1997), *Microphysics of Clouds and Precipitation*, pp. 954 , D. Reidel, Dordrecht, Netherlands.
Rienecker, M. M., et al. (2008), The GEOS-5 data assimilation system—Documentation of versions 5.0.1, 5.1.0, and 5.2.0, in *Tech. Rep. NASA/TM-2008-104606*, Goddard Space Flight Center, Greenbelt, Md.
Rosenfeld, D., R. Lahav, A. Khain, and M. Pinsky (2002), The role of sea spray in cleansing air pollution over ocean via cloud processes, *Science*, *297*(5587), 1667–1670.
Rosenfeld, D., H. L. Wang, and P. J. Rasch (2012), The roles of cloud drop effective radius and LWP in determining rain properties in marine stratocumulus, *Geophys. Res. Lett.*, *39*, L13801, doi:10.1029/2012GL052028.
Russell, L. M., et al. (2013), Eastern Pacific emitted aerosol cloud experiment, *Bull. Am. Meteorol. Soc.*, *94*(5), 709–729.
Sorooshian, A., S. Hersey, F. J. Brechtel, A. Corless, R. C. Flagan, and J. H. Seinfeld (2008), Rapid, size-resolved aerosol hygroscopic growth measurements: Differential aerosol sizing and hygroscopicity spectrometer probe (DASH-SP), *Aerosol Sci. Technol.*, *42*(6), 445–464.
Sorooshian, A., G. Feingold, M. D. Lebsock, H. L. Jiang, and G. L. Stephens (2009), On the precipitation susceptibility of clouds to aerosol perturbations, *Geophys. Res. Lett.*, *36*, L13803, doi:10.1029/2009GL038993.
Sorooshian, A., G. Feingold, M. D. Lebsock, H. L. Jiang, and G. L. Stephens (2010), Deconstructing the precipitation susceptibility construct: Improving methodology for aerosol-cloud precipitation studies, *J. Geophys. Res.*, *115*, D17201, doi:10.1029/2009JD013426.
Sorooshian, A., Z. Wang, G. Feingold, and T. S. L'Ecuyer (2013), A satellite perspective on cloud water to rain water conversion rates and relationships with environmental conditions, *J. Geophys. Res. Atmos.*, *118*, 6643–6650, doi:10.1002/jgrd.50523.
Sorooshian, A., G. Prabhakar, H. Jonsson, R. K. Woods, R. C. Flagan, and J. H. Seinfeld (2015), On the presence of giant particles downwind of ships in the marine boundary layer, *Geophys. Res. Lett.*, *42*, 2024–2030, doi:10.1002/2015GL063179.
Szumowski, M. J., R. M. Rauber, and H. T. Ochs III (1999), The microphysical structure and evolution of Hawaiian rainband clouds. Part III: A test of the ultragiant nuclei hypothesis, *J. Atmos. Sci.*, *56*, 1980–2003.
Takahashi, T. (1976), Warm rain, giant nuclei and chemical balance—A numerical model, *J. Atmos. Sci.*, *33*(2), 269–286.
Teller, A., and Z. Levin (2006), The effects of aerosols on precipitation and dimensions of subtropical clouds: A sensitivity study using a numerical cloud model, *Atmos. Chem. Phys.*, *6*, 67–80.
Terai, C. R., R. Wood, D. C. Leon, and P. Zuidema (2012), Does precipitation susceptibility vary with increasing cloud thickness in marine stratocumulus?, *Atmos. Chem. Phys.*, *12*(10), 4567–4583.
Terai, C. R., R. Wood, and T. L. Kubar (2015), Satellite estimates of precipitation susceptibility in low-level marine stratiform clouds, *J. Geophys. Res. Atmos.*, *120*, 8878–8889, doi:10.1002/2015JD023319.
Wang, Z., A. Sorooshian, G. Prabhakar, M. M. Coggon, and H. H. Jonsson (2014), Impact of emissions from shipping, land, and the ocean on stratocumulus cloud water elemental composition during the 2011 E-PEACE field campaign, *Atmos. Environ.*, *89*, 570–580.
Wang, Z., et al. (2016), Contrasting cloud composition between coupled and decoupled marine boundary layer clouds, *J. Geophys. Res. Atmos.*, *121*, 11,679–11,691, doi:10.1002/2016jd025695.
Wood, R., T. L. Kubar, and D. L. Hartmann (2009), Understanding the importance of microphysics and macrophysics for warm rain in marine low clouds. Part II: Heuristic models of rain formation, *J. Atmos. Sci.*, *66*(10), 2973–2990.
Woodcock, A. H. (1953), Salt nuclei in marine air as a function of altitude and wind force, *J. Meteorol.*, *10*, 362–371.
Woodcock, A. H., and M. M. Gifford (1949), Sampling atmospheric sea salt nuclei over the ocean, *J. Mar. Res.*, *8*, 177–197.
Woodcock, A. H., R. A. Duce, and J. L. Moyers (1971), Salt particles and raindrops in Hawaii, *J. Atmos. Sci.*, *28*, 1252–1257.
Yin, Y., Z. Levin, T. G. Reisin, and S. Tzivion (2000), The effects of giant cloud condensation nuclei on the development of precipitation in convective clouds—A numerical study, *Atmos. Res.*, *53*(1–3), 91–116.
Zhang, L. M., D. V. Michelangeli, and P. A. Taylor (2006), Influence of aerosol concentration on precipitation formation in low-level, warm stratiform clouds, *J. Aerosol Sci.*, *37*(2), 203–217.